X線分析の進歩 第 43 集（2012）抜刷
Advances in X-Ray Chemical Analysis, Japan, 43 (2012)
アグネ技術センター
ISSN 0911-7806

X-Ray Reflection Tomography Reconstruction for Surface Imaging: Simulation Versus Experiment

Vallerie Ann INNIS-SAMSON, Mari MIZUSAWA and Kenji SAKURAI

X-Ray Reflection Tomography Reconstruction for Surface Imaging: Simulation Versus Experiment

Vallerie Ann INNIS-SAMSON[*], Mari MIZUSAWA[**,***] and Kenji SAKURAI[*,**,#]

[*] University of Tsukuba
1-1-1 Tennodai, Tsukuba, Ibaraki 305-8577, Japan
[**] National Institute for Materials Science (NIMS)
1-2-1 Sengen, Tsukuba, Ibaraki 305-0047, Japan
[***] Comprehensive Research Organization for Science and Society (CROSS)
Tokai, Ibaraki 319-1106, Japan
[#] Corresponding author

(Received 22 January 2012, Revised 11 February 2012, Accepted 11 February 2012)

In this paper, we report the feasibility of X-ray reflection tomography to image patterned surfaces *via* simulation and experiment. In the simulation work, we were able to obtain very good reconstructed images from reflectivity projections with high correlation coefficient values obtained. Even with just 18 projections with a sinusoidal filter in the reconstruction algorithm, a high degree of colocalization was achieved. The spatial resolution obtained is 200 μm for a 24 μm detector resolution. Experimentally, we were able to obtain a successful reconstruction from at most 36 projections using an ordinary lab-source X-ray reflectivity set-up. Correlation coefficient values obtained are acceptable and yet can still be improved by upgrade of instrumentation design and the need for further mathematical processes in the FBP reconstruction algorithm. Spatial resolution currently obtained is ~1.6 mm. Further improvements are being done to have a comparable resolution with that of simulation.

[Key words] X-ray reflectivity, Imaging, Inhomogeneous sample, Patterns, Tomography

1. INTRODUCTION

We reported previously [1], a novel surface imaging technique which we called *X-ray reflection tomography* for imaging heterogeneous structures found on surfaces. With X-ray reflection tomography, the forward specular reflection from the reflecting surface at grazing incidence is being recorded and by rotating the sample in-plane, reflectivity line integral projections can be used to reconstruct the two-dimensional pattern or heterogeneous structures on the surface. The advantages of using X-ray reflectivity for such projection-type reconstructive imaging include: 1) No need of high intensity X-rays to obtain data at near surface layers of dense materials like metals since reflectivity is used and not absorption. 2) Measuring time is much shorter especially if incident angle is near the critical angle of the sample because of whole area illumination. It is more efficient than point-by-point scanning [2]. 3) Beam hardening effects are avoided with the use of monochromatic X-ray sources in XRR. 4) Resolution of XRR along the depth is in the order of a few angstroms (1A) compared to normal absorption X-ray CT which is in the millimeter to

sub-millimeter range [3]. This is advantageous for imaging structures at near surface layers (*e.g.* a few hundred angstroms under the surface) without slicing the sample for thin films and multi-layered materials (*e.g.* semiconductor devices).

To reconstruct the patterns/structures on the surface, just like X-ray computer tomography [4], reconstructive algorithms are utilized. The idea of reconstruction is based on the Radon transform [5] as a series of line integrals through $f(x,y)$ at different offsets from the origin, whereby the projections $p_\theta(u)$, where u is a point on the projection axis, is related to the reflectivity edge map $f(x,y)$ by :

$$p_\theta(u) = \int_{-\infty}^{\infty}\int_{-\infty}^{\infty} f(x,y)\delta(x\cos\theta + y\sin\theta - u)dxdy \quad (1)$$

Thus by performing a 1-D Fourier transform on the projection followed by a 2-D inverse Fourier transform, which is the Fourier slice theorem, a reconstruction of the surface is done.

In our technique, the filtered back-projection (FBP) algorithm was used to perform the reconstruction. The FBP algorithm is also based on the Fourier slice theorem and it inverts Eq. (1) to recover $f(x,y)$ by first filtering the projection data with a filter kernel then backprojecting it across the image plane. The filter kernel removes the blurring in simple backprojection (due to summation of "tail" artifacts from the projections) and results in a mathematically exact reconstruction of the image. An image is reconstructed by summing all the resulting filtered backprojections. This algorithm for image reconstruction from projections is common in Computer Tomography (CT) as it is computationally efficient [4].

Prior to actual experimental work on XRR tomography, simulation work was carried out. The use of simulation is necessary prior to experimentation to have an understanding of how various parameters can influence/contribute to the reconstructed image quality. By comparing the results from the experiment, there is a better understanding of what factors need to be improved to have results similar to that of the simulation.

We report here our simulation work of X-ray reflection tomography using a phantom image as well as a direct comparison of the reconstruction of an actual sample *via* experiment.

2. MATERIALS AND METHODS

Simulation Scheme:

We first set-up a phantom surface (10 cm × 10 cm dimensions) with materials of different reflectivity as shown in Fig.1a. A phantom is a test object/image to simulate the projections and the quality of the reconstruction algorithm. A reflectivity value R (which depends on the material and the incident angle of the X-ray source to the sample) was assigned at each point (x,y) on the surface. We assume a parallel beam projection (X-rays travel only in a straight path) such that the reflectivity projection, $p(\theta, y_n)$, for a particular projection angle θ, at a point y_n of the detector is just taken to be:

$$p(\theta, y_n) = \sum_m \frac{R(x_m, y_n)}{i} \quad (2)$$

where i is the number of cell elements in the row. The parallel beam projection geometry [6] is also suitable since experimentally we have an X-ray line source. The reflectivity projection is thus a 1-D data along the y-axis. The phantom surface is rotated equidistantly (*e.g.* 2º, 5º, 10º) for a 180º range and the reflectivity projection is taken at each projection angle. A projection on the y-z plane is formed by combining all the line integrals at each angle. A collection of the reflectivity projection data for all projection angles is shown as a sinogram in Fig.1(b) in 8-bit gray-scale. With the use of FBP algorithm,

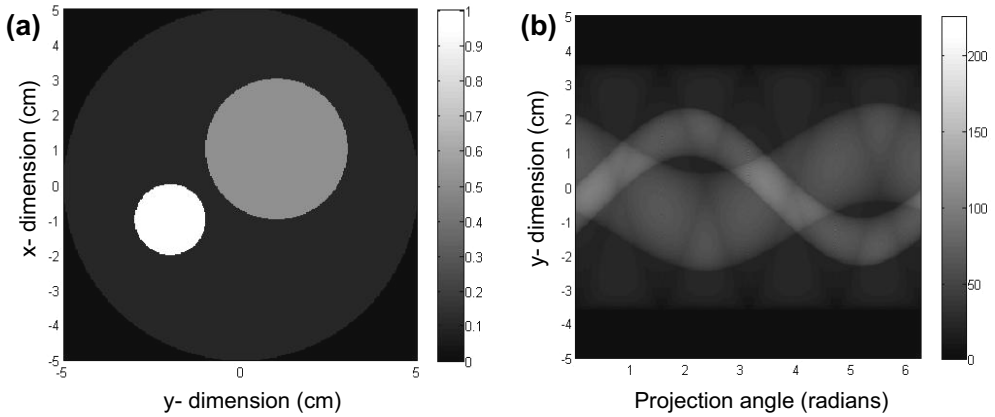

Fig.1 (a) Phantom surface showing a material with different reflectivity. The *x*- and *y*- axes are the dimensions of the phantom (in centimeters) and the brightness/darkness of the surface relates to the reflectivity of the surface. The reflectivity spectrum is shown on the right side. (b) Simulated reflectivity projections from the surface are shown in a sinogram.

reconstruction of the phantom image from the reflectivity projection data was done. The type of filter used in the FBP algorithm was varied to see the effects on the reconstructed image. All simulations were done using MATLAB programming language.

Sample Preparation:

Sputtering on pre-cleaned SiO/Si substrate was done by an Emtech SC7620 sputter coater using gold as target. Si substrate (size: 2.5 cm × 2.5 cm) was put inside the coater and a mylar mask with the cut pattern was put on top of the Si. Gold was used because of its high reflectivity coefficient contrast with the Si substrate at a certain angle.

Equipment:

The set-up is mainly a RIGAKU Rint-ATX system used for reflection and diffraction measurements. We built a specialized image plate holder in front of the sample since an image plate (IP) was used as a detector. We have previously described our set-up in [1]. For the measurements, X-ray source power is set at the lowest power 20 kV × 10 mA as a compromise with the counting time so as not to saturate the image plate. For each ϕ angle, reflection is recorded for 30 seconds in the IP (with resolution of 50 μm) and data from the IP is read by an image plate reader. The image data is processed by the image software tool Image-Pro Plus. Reconstruction of the data is done *via* FBP algorithm written also in MATLAB.

3. RESULTS AND DISCUSSION

3.1 Simulation Results:

Fig.2 shows the calculated reconstruction of the phantom surface in Fig.1, *via* filtered-back projection algorithm. Fig.2a-d are the reconstructed images with increasing number of projection angles used in the reconstruction. As shown in the figures, the image reconstruction quality becomes better with increase in the number of projection angles used, as expected. To quantitatively evaluate the image quality of the reconstructed images using the FBP algorithm, the following two measures were used to quantify the reconstruction accuracy [7]:

(1) Pearson's correlation coefficient (PCC):

$$r = \frac{\sum_i (s1_i - s1_{ave}) \times (s2_i - s2_{ave})}{\sqrt{\sum_i (s1_i - s1_{ave})^2 \times (s2_i - s2_{ave})^2}} \quad (3)$$

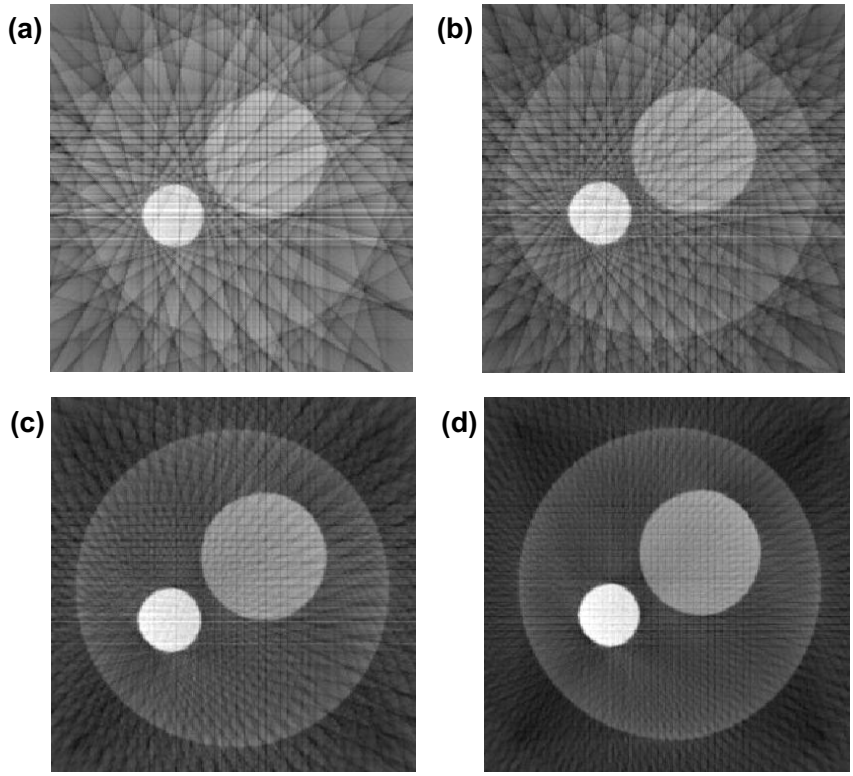

Fig.2 Simulated XRR tomography reconstructions for the phantom in Fig.1, done *via* FBP algorithm are shown in (a) for 12 projections, in (b) for 18 projections, in (c) for 36 projections, and in (d) for 60 projections.

(2) Mander's overlap coefficient (MOC):

$$r = \frac{\sum_i s1_i \times s2_i}{\sqrt{\sum_i (s1_i)^2 \times (s2_i)^2}} \qquad (4)$$

The value $s1$ is the signal intensity from image 1 while $s2$ is the signal intensity from image 2 at each image pixel i. $s1_{ave}$ and $s2_{ave}$ are the mean intensities for each image. The two measures are mathematically similar, differing only in the use of either the absolute intensities (MOC) or the departure from the mean (PCC) in both the numerator and the denominator. The denominator acts to limit the range of the coefficients: 0 to +1 for the MOC and –1 to +1 for the PCC. r value of 0 signifies no overlap and 1 represents complete image overlap for MOC. For PCC, +1 is for perfect correlation, –1 is perfect but negative correlation and 0 denoting the absence of a relationship. Shown in Table 1 are the MOC and PCC values for the 4 reconstructed images in Fig.2 versus the phantom image.

Quantitatively, the correlation coefficient and the overlap coefficient values increase with the number of projection angles used. At 12 and 18 projection angles, streak artifacts from the back-projection, are clearly observed on the reconstructed image (see Figs.2a and 2b). The lines have darker intensities on the edges thus make the intensities on the reconstructed surface non-uniform. These

Table 1 Mander's overlap coefficient values (MOC) and Pearson correlation coefficient (PCC) values for the reconstructed image and the phantom object for different number of projection angles used in the reconstruction.

No. of projections	MOC	PCC
12	0.814	0.695
18	0.845	0.750
36	0.876	0.804
60	0.896	0.835

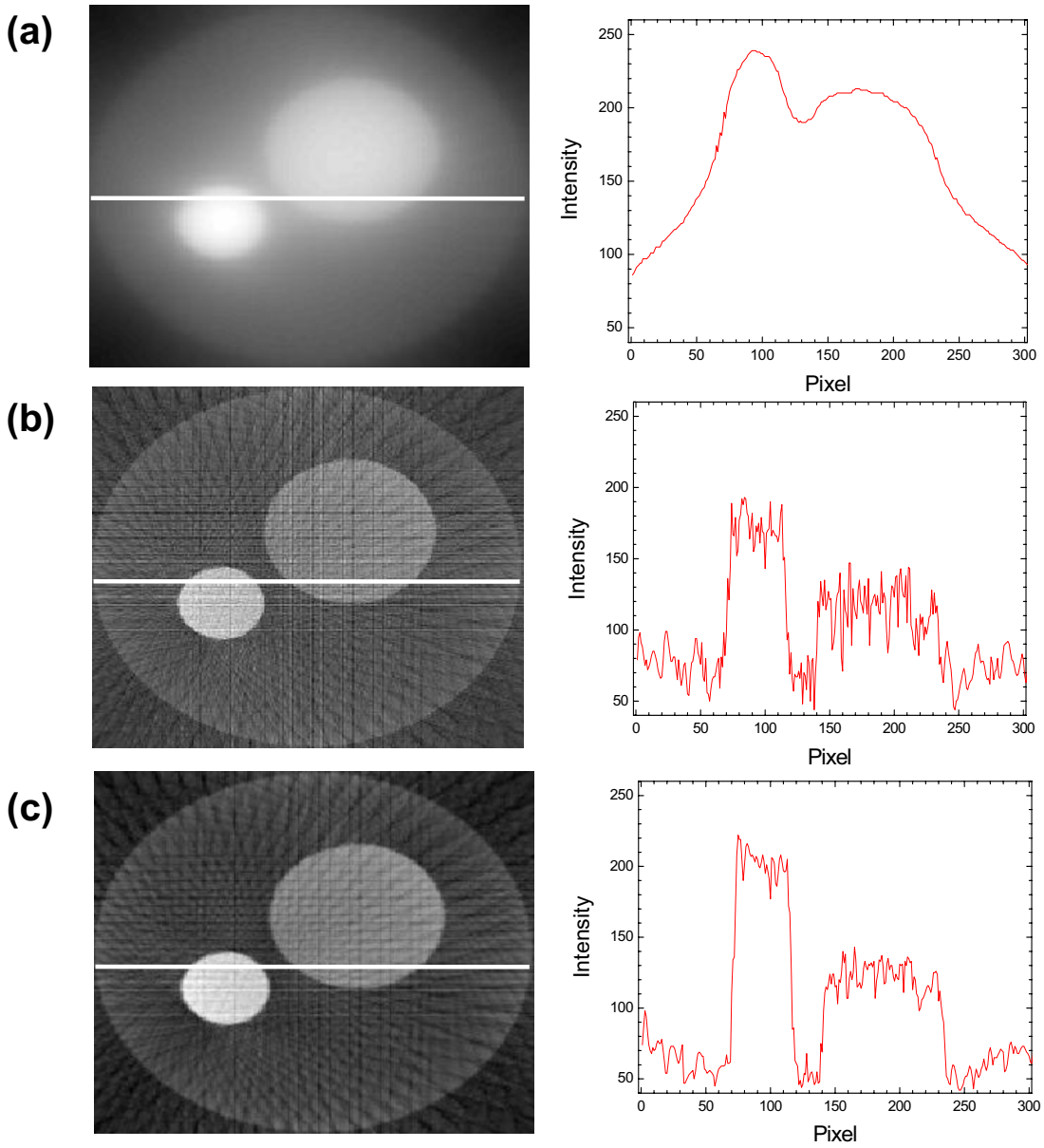

Fig.3 Reconstructed images for the phantom in Fig.1 with different filter functions used in the FBP algorithm reconstruction. (a) Low-pass filter, (b) High-pass filter, (c) Sinusoidal filter. Intensity profile along the white line of each image is shown on the right side to emphasize the effect of the filter function on the intensities of the reconstructed image.

artifacts contribute to the low PCC values since PCC can give negative values if the deviation from the average signal intensity is large. MOC is not sensitive to intensity variations in the image analysis thus it has usually higher values than PCC. Nevertheless, a correlation coefficient higher than 0.75 was obtained and such coefficient values are considered to be a relatively high degree of colocalization.

By using different filter functions on the FBP algorithm, the quality of the reconstructed image will also change as shown in Fig.3. Because

Table 2 Mander's overlap coefficient values (MOC) and Pearson correlation coefficient (PCC) values for the reconstructed image and the phantom object using different filter functions in the FBP algorithm reconstruction (36 projection angles used).

Filter function	MOC	PCC
Low-pass	0.786	0.732
High-pass	0.750	0.750
Sinusoidal	0.876	0.804

of the different functions of such filters, Fig.3a shows a smoother image of the reconstructed object for the low-pass filter, while Fig.3b shows more emphasized edges of the image for the high-pass filter. This observation can also be seen in the intensity profile of the line drawn across the images. The sinusoidal filter gives the best reconstruction among the three as the edges are clearly defined but less high frequency components. Intensity values for the low-pass filtered reconstruction showed higher intensity (on an 8-bit gray-scale level) as compared to the 2 other filters.

Quantitatively, FBP algorithm with the use of a sinusoidal filter gives the highest MOC and PCC values as compared to the 2 other filter functions. The PCC and MOC values of the reconstructed image versus the phantom object are shown in Table 2. Because of the high MOC and PCC values with the sinusoidal filter, it was the preferred filter for reconstructing the experimentally obtained projection data.

The spatial resolution obtained is around 200 μm for 1024 × 1024 pixel elements used (or a detector resolution of 28 μm) in the simulation. The algorithm can resolve reflectivity differences as low as 0.01 for low reflectivity materials while for high reflectivity materials, it can resolve reflectivity differences of 0.1.

3.2 Experimental Results:

Shown in Fig.4 are the reconstructed images of an actual patterned sample (University of Tsukuba logo) wherein the experimental projection data was obtained *via* XRR tomography. The sinusoidal filter was used in the FBP algorithm reconstruction as it gave the best reconstruction in the simulation results. As shown in Fig.4b, reconstruction with only 7 projections gives an unrecognizable image with the large amount of streak artifacts. These artifacts are due to noise or poor signal-to-noise ratio, undersampling, strong scattering around the edges of the sample and diffuse scattering component of the reflectivity which cannot be cut-off in our experimental set-up. With increasing the number of projections, the undersampling artifact is decreased thus a clearer image can be produced (Figs.4c and 4d). The smallest interval angle between projections was 5º, and the angular range was 0º - 180º, thus the number of projections used in the reconstruction was 7, 19 and 37 projections respectively. The PCC and MOC values of the reconstructed image for the varying number of projections are shown in Table 3.

Compared to the simulation results, the PCC values obtained from experimental results are lower due to the artifacts mentioned previously. PCC is sensitive to the intensity variations thus the lower values. Considerable graining is still observed in the reconstructed image from 37 projections due to noise artifact or a poor signal-to-noise ratio which gives a not so high PCC value. We usually set the power to the lowest value to avoid saturation of the image plate detector and the measurement time is set to 30s. The detector is also placed at a considerable distance from the sample due to limitation of the instrumentation geometry. Further optimization is currently being done to increase the signal-to-noise ratio and avoid such ar-

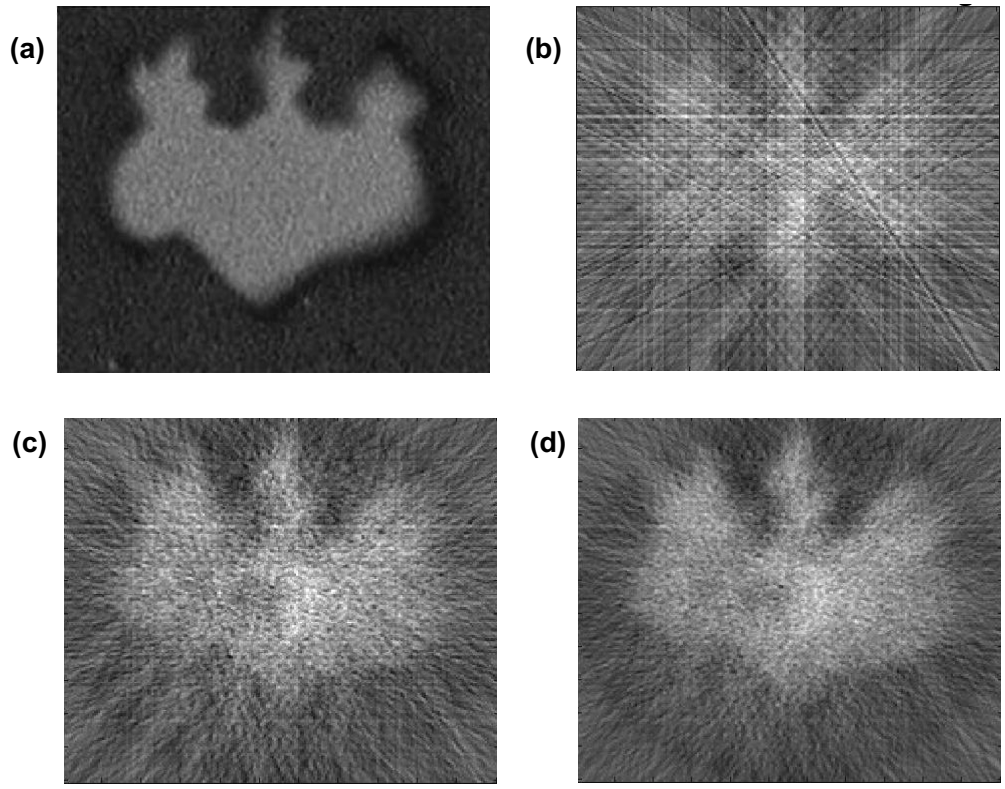

Fig.4 Image of actual sample in gray-scale and the reconstructed images *via* XRR tomography for (a) 7 projections, for (b) 19 projections, and for (c) for 37 projections.

Table 3 Mander's overlap coefficient values (MOC) and Pearson correlation coefficient (PCC) for the reconstructed image and the phantom object for different number of projection angles used in the reconstruction.

No. of projections	MOC	PCC
7	0.839	0.434
19	0.869	0.573
37	0.883	0.636

tifact in the reconstruction. This will also increase our current spatial resolution. Strong scattering along the edges are also seen in the image because of the thicker coating on the edges of the pattern.

We tried to apply different filters to the reconstructed image to increase the correlation coefficients and to obtain a better reconstruction. Shown in Fig.5 are the reconstructed images with their respective intensity profile along the line drawn. Image of the actual sample was also included for comparison. Similar to the simulation results, using an LP filter produces a rounding of the intensity curve and a low contrast between the high reflectivity and low-reflectivity part. The high-pass filter on the other hand gave a very poor contrast between the high reflectivity and low-reflectivity part and a noisy intensity profile. The sinusoidal filter gave a better contrast with less noise. The PCC and MOC values are shown in Table 4 and it showed that the high-pass filter gave the lowest PCC and MOC values, as expected from its intensity profile. Unlike the simulation results, the low-pass filtered reconstruction gave the highest PCC and MOC values which may be due to the smooth intensity profile wherein the deviation of

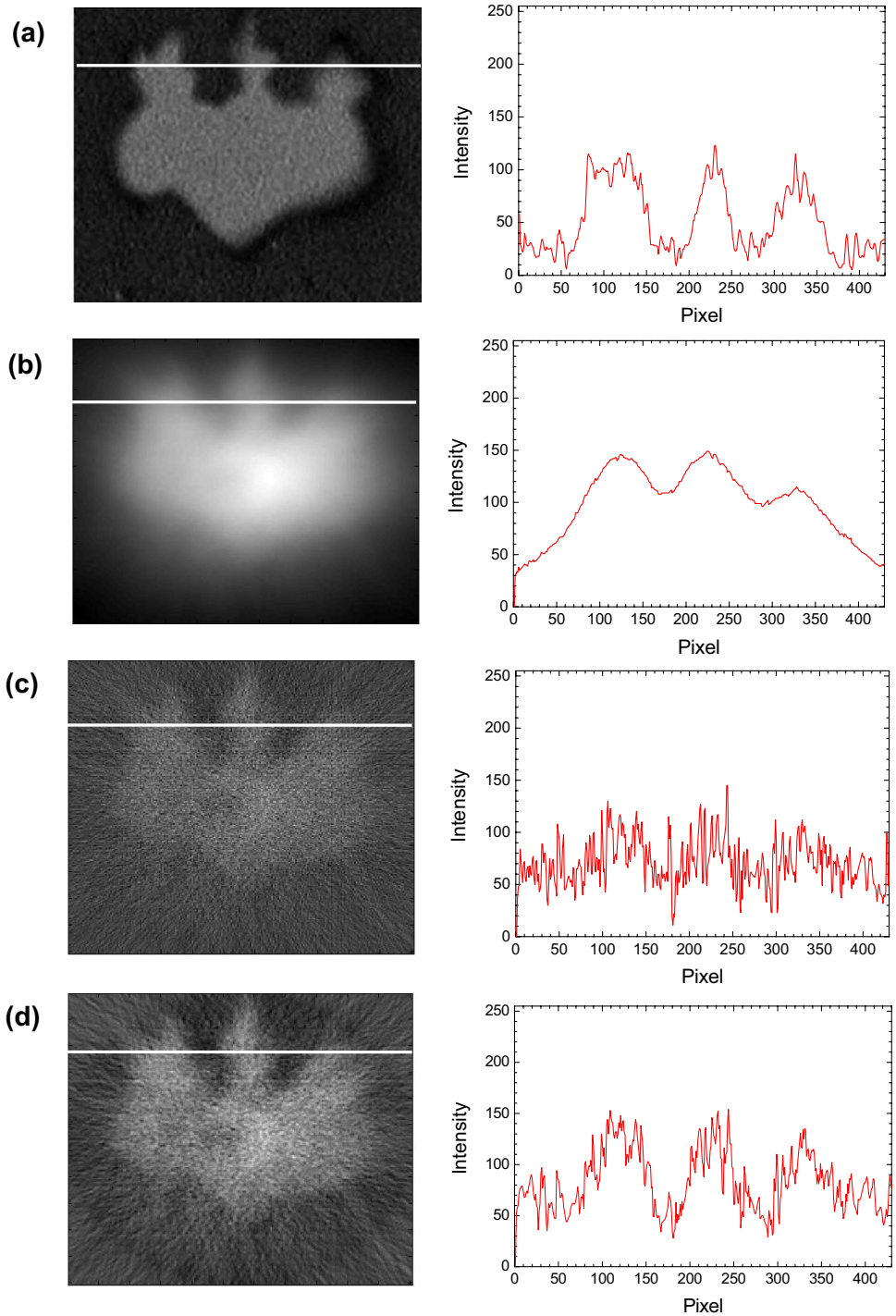

Fig.5 (a) Image of actual sample (gray-scale, 8-bit) with its intensity profile along the red line. (b-d) Reconstructed images for the patterned sample using different filter functions in the FBP algorithm reconstruction. (b) Low-pass filter (c) High-pass filter (d) Sinusoidal filter. Intensity profile along the white line of each image is shown on the right side to emphasize the effect of the filter function on the intensities of the reconstructed image.

Table 4 Mander's overlap coefficient values (MOC) and Pearson correlation coefficient (PCC) values for the reconstructed image and the patterned sample using different filter functions in the FBP algorithm reconstruction (37 projection angles used).

Filter function	MOC	PCC
Low-pass	0.908	0.735
High-pass	0.836	0.417
Sinusoidal	0.883	0.636
Sinusoidal + low-pass filter image processing	0.907	0.764

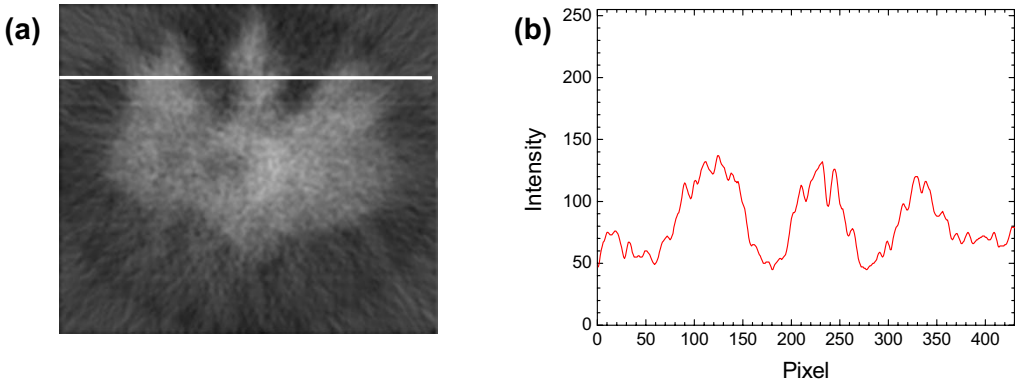

Fig.6 Smoothing was applied to the reconstructed image in Fig.5d *via* low-pass image filter and the resulting image is (a) and the intensity profile along the white line is (b).

the intensities from the average intensity, at each point, is not large. By performing a smoothing on the reconstructed image from sinusoidal filter *via* low-pass filter, the PCC value is improved and a very minimal decrease in MOC value due to intensity changes is obtained. The intensity profile shows attenuated high-frequency components on the curve after smoothing (See Fig.6).

Further improvements are underway to improve the reconstruction ability by decreasing the streak artifacts seen in the images. This can be done by improving our current set-up to remove the diffuse scattering component of the reflectivity as well as the strong scattering component. The current experimental resolution of ~1.6 mm (for a 50 μm detector resolution) is also due to the limitation of the set-up and this also needs to be reduced further to see finer details on the surface. Although filtered back-projection algorithm gave acceptable PCC and MOC values of the reconstructed image, further mathematical process (*e.g* interpolation) should be applied to the image to decrease the streak artifacts. At present, the limit of the number of projections obtained experimentally is 36 due to actual time consumed in the measurement. Efforts are being done to increase the projection number, without too much experimental time consumed, to have better reconstruction.

4. CONCLUSIONS

By simulating its reflectivity projections, we were able to successfully reconstruct a phantom image *via* simple filtered-back projection algorithm. With just 18 projections, relatively high colocalization with the original image was obtained as shown in

the correlation coefficient values. The use of a sinusoidal filter function in the reconstruction algorithm gave the best reconstruction. The spatial resolution obtained is 200 μm for a 24 μm detector resolution.

Using an ordinary lab-source X-ray reflectivity set-up, we performed our XRR tomography experiments with a gold-patterned sample on a Si substrate. Gold was used because of its high reflectivity and its high reflectivity coefficient contrast with the Si substrate at a particular incidence angle. With just 36 projections, successful reconstruction was obtained which captures most of the details of the outside edges with acceptable colocalization. Unlike simulation results, simple FBP algorithm may not be enough to obtain a high degree of colocalization of the actual sample and the reconstructed image. Further mathematical processing or image processing needs to be done to improve the image quality. Current spatial resolution is 1.6 mm (with an IP resolution of 50 μm) as reported previously [1)] and instrumental and calculation improvements are underway to increase the resolution.

References

1） V.A.I. Samson, M. Mizusawa, K. Sakurai, *Anal. Chem*., 2011, **83**(20), 7600-7602.

2） K. Sakurai, M. Mizusawa, M. Ishii, S. Kobayashi, Y. Imai, *J. Phys*.: *Conference Series*, 2007, **83**, 012001.

3） S. Ulzheimer, T.Flohr, "Multislice CT: Current Technology and Future Developments" in Multislice CT (Springer-Verlag, Berlin, Heidelberg, 2009) Chapter 1.

4） G.T. Herman, Image Reconstruction from Projections: The Fundamentals of Computerized Tomography (Academic Press, New York-London, 1980) Chaps. 1-2.

5） M. Born, E. Wolf, Principles of Optics (Cambridge Univ. Press, UK, 1999) Chapter 4.

6） A.C. Kak, M.Slaney: Principles of Computerized Tomographic Imaging (IEEE Press, New York, 1988) Chap. 8.

7） E.M.M. Manders, F.J. Verbeek, J.A. Aten, *J. Microscopy*, 1993, **169**, 375-382.